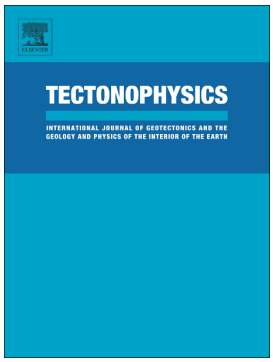

Stress field and active faults in the orogenic front of the Andes in the Malargüe fold-and-thrust belt (35°–36°S)

J.F. Mescua, M. Barrionuevo, L. Giambiagi, J. Suriano, S. Spagnotto, E. Stahlschmidt, H. de la Cal, J.L. Soto, M. Mazzitelli

PII: S0040-1951(19)30228-8
DOI: https://doi.org/10.1016/j.tecto.2019.06.003
Reference: TECTO 128133

To appear in: *Tectonophysics*

Received date: 29 December 2018
Revised date: 26 May 2019
Accepted date: 3 June 2019

Please cite this article as: J.F. Mescua, M. Barrionuevo, L. Giambiagi, et al., Stress field and active faults in the orogenic front of the Andes in the Malargüe fold-and-thrust belt (35°–36°S), Tectonophysics, https://doi.org/10.1016/j.tecto.2019.06.003

Stress field and active faults in the orogenic front of the Andes in the Malargüe fold-and-thrust belt (35°-36°S)

J.F. Mescua[1,2], M. Barrionuevo[1], L. Giambiagi[1], J. Suriano[1], S. Spagnotto[3], E. Stahlschmidt[4], H. de la Cal[5], J.L. Soto[5], M. Mazzitelli[1]

1. Instituto Argentino de Nivología, Glaciología y Ciencias Ambientales (IANIGLA), CCT Mendoza, CONICET
2. Facultad de Ciencias Exactas y Naturales, Universidad Nacional de Cuyo
3. CONICET–Departamento de Física, Universidad Nacional de San Luis
4. El Trébol S.A.
5. Roch S.A.

Abstract

We integrate field and wellbore data to discuss the stress field in the frontal sector of the Malargüe fold-and-thrust belt (Andes of Argentina). Surface observations indicate N-S thrusts and NW to WNW and ESE strike-slip faults are active in the study area. Inversion of fault kinematic indicators, combined with borehole breakout data and a mini-frac test within the study area, constrain the Quaternary to recent stress state, which is characterized by a subhorizontal, E-W oriented maximum stress, and by intermediate and minimum stresses with similar magnitudes that are locally interchanged, producing a setting in which reverse and strike-slip faults are alternatively active. The implications of the recognized structures for earthquake hazard are examined.

Keywords: Active faults; crustal stress; Andes

1. Introduction

The development of fold-and-thrust belts in orogenic environments is the result of contraction, which is usually interpreted as a result of a compressional stress state, with the minimum principal stress (σ_3) in the vertical direction. In this stress regime, thrusts and reverse faults are active (Anderson, 1951) with trends sub-perpendicular to the horizontal maximum principal stress (σ_1). In particular, during advance of the orogenic wedge, the active frontal structures are usually assumed to be orogen parallel thrusts (e.g. Elliot, 1976; Chapple, 1978).

However, as Lacombe *et al.* (2010) and Tavani *et al.* (2015) noted, the occurrence of transversal structures (strike-slip or more rarely normal faults) in the frontal sector of fold-and-thrust belts is frequent. Field and microstructural analyses suggest that the intermediate principal stress (σ_2) is vertical during the development of these structures and the minimum principal stress (σ_3) is horizontal, giving place to what these authors call the "σ_2 paradox" (Tavani *et al.*, 2015).

In this work, we study the orogenic front of the Malargüe fold-and-thrust belt in the Andes of Argentina (35-36ºS, Fig. 1). The Pliocene-Quaternary stress state in this region is debated in recent works, with some researchers proposing an extensional regime (Ramos and Kay, 2006; Folguera *et al.*, 2008, 2009), while others reported active thrust faults (Silvestro *et al.*, 2005; Giambiagi *et al.*, 2008) suggesting compression.

We document N-trending thrusts that constitute the main structures in the study area, placing Cretaceous rocks over Quaternary deposits. Thrusts are locally displaced tens of meters by NW, WNW and ESE-trending strike-slip faults, some of which juxtapose Cretaceous rocks and Quaternary desposits. We explore the possible setting in which both kinds of structures could be active and their implications for seismic hazard.

2. Geologic setting

The Malargüe fold-and-thrust belt is a basement-involved belt developed in the eastern side of the Andes between 34° and 36°S (Fig. 1). In this region, the basement corresponds to the Late Permian-Early Triassic acidic volcanic rocks of the Choiyoi Group (Llambías *et al.*, 1993). The sedimentary cover consists of Late Triassic-Paleocene deposits of the Neuquén basin, a retroarc basin filled with alternating marine and continental sediments that reach thicknesses over 6.000 m in the most important depocenters (Legarreta and Uliana, 1999). The evolution of the basin is characterized by a Late Triassic-Early Jurassic extensional event, during which depocenters controled by NNE- and NNW-trending normal faults were developed at the latitude of the study area (Legarreta and Uliana, 1999; Giambiagi *et al.*, 2009). The Middle Jurassic-Early Cretaceous was dominated by thermal subsidence (Legarreta and Gulisano, 1989), with an episode of normal fault reactivation in the Late Jurassic (Cegarra and Ramos, 1996; Charrier *et al.*, 2017; Mescua *et al.*, 2008). During the Late Cretaceous, Andean uplift began and the Neuquén basin became a foreland basin (Mpodozis and Ramos, 1989; Tunik *et al.*, 2010). The latest Cretaceous to Paleocene fill of the basin corresponds to the first Atlantic marine ingression (Legarreta and Uliana, 1999).

The final uplift of the Andes took place since 20 Ma, as recorded by Miocene to recent synorogenic deposits locally preserved within the thrust belt (*e.g.* Silvestro *et al.*, 2005). This orogenic stage is characterized by a progression of deformation

towards the foreland since the middle Miocene (Mescua *et al.*, 2014), with the main structuration of the orogenic front (Fig. 1) taking place since 7 Ma in the northern part of the study area (Malargüe anticline, Silvestro *et al.*, 2005). In the southern part of the study area, the orogenic front was uplifted earlier (17 Ma at Sierra de Palauco, Silvestro and Atencio, 2009). Out of sequence activity in thrusts of the inner sector of the belt took place although its age is not well constrained (Kozlowski *et al.*, 1993; Mescua *et al.*, 2014). The main structures along the orogenic front are

thrusts and reverse faults, with associated fault-related folds. Dominant east-vergent basement structures transfer shortening to the cover with detachment levels in shale and gypsum units (Kozlowski *et al.*, 1993). Locally, west-vergent thrusts developed giving place to triangle zones (Manceda and Figueroa, 1995; Silvestro and Atencio, 2009). Traverse structures, oblique to the strike of the orogen, have been recognized throughout the belt. These faults are usually interpreted as structures developed during the Late Triassic-Early Jurassic extensional episode and inverted during Andean orogenesis (e.g. Yagupsky *et al.*, 2008; Bechis *et al.*, 2010). Boll *et al.* (2014) related WNW-trending faults to inherited structures and interpreted ENE faults as opening fractures parallel to the direction of maximum horizontal stress during Andean orogenesis, and proposed that these structures were active between the Late Cretaceous and the late Miocene.

The Pliocene to Quaternary stress field has been the subject of debate in recent works. Some researchers suggested extension as a result of orogenic collapse of the Andes, proposing active normal faults (Ramos and Kay, 2006; Folguera *et al.*, 2008, 2009). In contrast, Silvestro *et al.* (2005) indicate activity of the Malargüe fault and uplift of the Malargüe anticline between 7 and 1 Ma (Fig. 1), and Giambiagi *et al.* (2008) document thrusting of Paleocene rocks over Pleistocene deposits in the Sosneado fault near the town of El Sosneado (Fig. 1).

3. Methods

We consider that structures that affect Pliocene-Quaternary sediments are active faults. These structures were recognized from published maps and satellite images and verified in the field. During fieldwork, we determined the affected units, measured bed orientations and measured kinematic indicators on minor faults (cm to m of displacement) associated with the thrusts and strike-slip faults. Kinematic data was obtained from slickensides (direction of movement) and

displacement of marker beds, mineral growth lineations and Riedel fractures (sense of movement). At each station, measurements vary between n=5 and n=20.

Kinematic data from faults were analyzed using the FaultKin software (Allmendinger, 2001). The software calculates P (contraction) and T (tension) axes for each datum and uses Linked Bingham statistics to calculate the aggregate deformation axes λ_1, λ_2 and λ_3.

The directions of the stress field components were obtained from borehole breakout data (Cox, 1970; Bell and Gough, 1982; Zoback *et al.*, 1985), and from the inversion of kinematic indicators from minor faults (Angelier, 1975, 1984, 1990; Lacombe, 2012).

Borehole logging reports on three wells were used to identify sections with breakouts (Cox, 1970; Bell and Gough, 1982; Zoback *et al.*, 1985). Breakouts are sections of the wellbore deformed by the stresses acting on the walls. The direction of the long section of the elliptic borehole can be measured and is interpreted to indicate the minimum horizontal stress (S_{hmin}) direction. Data quality was characterized using the World Stress Map classification (Sperner *et al.*, 2003).

Kinematic indicators were inverted for stress using the T-TECTO software (Zalohar and Vrabec, 2007) and the methods outlined in Giambiagi *et al.* (2016). We obtained reduced stress tensors that record the orientation of the principal stress (σ_1, σ_2 and σ_3) and the stress ratio $\phi = [(\sigma_2-\sigma_3)/(\sigma_1-\sigma_3)]$. The stress ratio permits to classify the stress regime defining compressional, strike-slip and extensional regimes and transitional states between them when two of the main stresses are similar in magnitude.

In order to estimate the magnitudes of stresses in the region, we combine a mini-frac test from an oilwell in the northern study area with geomechanical considerations, taking into account the results from the stress inversion. The mini-frac test provides a measurement of the value of σ'_3 (Zoback, 2010). In order to estimate σ'_1 we take into account the evidences of active faulting in the region. Considering that the friction coefficient (μ_s) of fractures limits the effective differential stress, and assuming $\mu_s = 0.6$ (Jaeger and Cook, 1979; Byerlee, 1978), we can use the relation:

$$\sigma'1/\sigma'3 \leq [(\mu^2+1)^{1/2}+\mu]^2 \sim 3.1$$

to estimate σ'_1 (Jaeger y Cook, 1979; Zoback y Townend, 2001).

On the other hand, we calculate the vertical stress σ_v integrating the densities of the rock column of a borehole with density log data and compare this value with the estimations of σ'_3 and σ'_1 to determine the current stress field.

With the determined stress field, we carried out a slip tendency analysis (Morris *et al.*, 1996) using the "Stress analysis" module implemented in the Move© software. This method consists in calculating the relationship between the normal and shear stress on planes of all orientations, obtaining a value between 0 and 1. Planes with a value of slip tendency over 0.6, the friction coefficient assumed as standard (Byerlee, 1978), correspond to planes that will slide, indicating active faults in the prescribed stress regime.

Finally, taking into account the active faults recognized in the region, we modeled the Coulomb static stress changes produced on the structures by earthquakes on the major thrusts of the area. This change is defined as

$$\Delta\sigma_f = \Delta\tau_\beta - \mu' \Delta\sigma_\beta$$

where $\Delta\sigma_f$ is the change is Coulomb stress, $\Delta\tau_\beta$ is the change in shear stress, μ' is the effective coefficient of friction and $\Delta\sigma_\beta$ is the change in normal stress (King *et al.*, 1994).

We used the Coulomb 3.2 software (Toda *et al.*, 2005; Lin and Stein, 2004) to calculate stress changes using different faults as sources with earthquake magnitudes according to their length (Wells and Coppersmith, 1994; Wesnousky, 2008; Leonard, 2010), always assuming a friction coefficient $\mu_s = 0.6$.

4. Active faults

4a. Northern sector

In the northern sector of the study area (Fig. 2), we studied three sectors where active structures could be recognized and characterized.

At Cerro Pencal (Figs. 2, 3), an active N-S-striking low-angle backthrust places Upper Cretaceous redbeds of the Neuquén Group (Cenomanian-Campanian, Tunik *et al.*, 2010) over Quaternary deposits, uplifting the Cerro Pencal hill (Figs. 2, 3). Quaternary deposits in the northern area correspond to polymictic conglomerates with subangular and subrounded clasts of up to 50 cm of diameter, locally containing larger clasts. Unfortunately no further constraints are available on the age of these deposits. The backthrust can be mapped for 5.5 km along strike, and its southern and northern ends are covered by alluvium. A minor east verging thrust affecting Quaternary deposits was also observed in this region (Fig. 4). The Cerro Pencal backthrust is segmented by 20 m-wide strike-slip fault zones composed of a series of minor subparallel faults (Fig. 3) with a few centimeters to 1.5 m of displacement, which accumulate tens of meters of displacement for the whole fault zone. Faults with WNW trend are sinistral, as shown by field relations and kinematic data (Fig. 3), while minor conjugate faults with ENE trend are dextral.

South of the Salado river, in Puesto Rojas (Fig. 2), a N-trending backthrust placing Upper Cretaceous redbeds over Quaternary deposits was also recognized, with a splay fault towards the west (Fig. 5). This structure could be the southern continuation of the Cerro Pencal backthrust, although it is uncertain if these structures constitute a single fault or two separate segments. The main fault strand can be recognized for 7 km along strike. The clearest evidence of recent activity of the strike-slip faults is found in Puesto Rojas, where WNW-trending sinistral fault that juxtaposes

mid-Cretaceous limestones (Huitrín Fm. of Albian age, Leanza, 2003) and Quaternary deposits (Fig. 5a). East of this structure, the same units are affected by an east-verging thrust (Fig. 5b). The easternmost active structure recognized in the area is an east-verging thrust that places Upper Cretaceous redbeds of the Neuquén Group over Quaternary (Fig. 5c). Associated with this structure, minor faults with 0.5 m of displacement affecting Late Cretaceous redbeds and Quaternary deposits also indicate active contraction and reverse faulting in this sector (Fig. 5d, e).

At Cerro Mollar (Figs. 2d and 6), mid-Cretaceous rocks are thrusted over Quaternary deposits along an east-verging structure. Poor exposure in this sector prevented us from determining the lateral extent of the fault. West of the thrust, WNW-trending faults corresponding to 40-50 m-wide zones of fracturing in Upper Cretaceous redbeds were observed. Analysis of kinematic data from these structures reveals a sinistral displacement, with minor or absent dip slip (Fig. 6).

The active thrusts that we recognized are linked to major blind reverse faults observed in seismic lines and wellbores (Kozlowski *et al.*, 1993; Rojas and Radic, 2002), the Malargüe (Fig. 1) and Puchenque (west of the study area) fault systems. These thick-skinned inverted Mesozoic normal faults are the main structures of the orogenic front of the Malargüe fold-and thrust belt at these latitudes (Fig. 7). The structural model proposed for the region suggests that these structures are also active.

4.b Southern sector

In the Cajón de los Caballos area (Figs. 1 and 8), poor exposures make the determination of cross-cutting relationship between structures difficult. Some N-trending thrusts in this sector (Fig. 8a) affect a volcaniclastic unit dated at 11-8 Ma (Loma Fiera Fm., Baldauf, 1993; Silvestro and Atencio, 2009; Horton *et al.*, 2016). Traverse WNW- and ESE-striking lineaments were recognized on

satellite images. Field observations indicate that these correspond to zones of fractures with strike-slip kinematic indicators (Fig. 8b). Cretaceous rocks are deformed close to the faults with beds rotated away from the regional N-trending attitudes. Satellite image interpretation suggests that strike-slip faults affect the younger rocks in the region (basalts dated at *ca.* 3-2 Ma, Silvestro and Atencio, 2009). We could only measure kinematic data on Late Cretaceous beds affected by WNW-trending strike-slip faults, showing sinistral displacement, and ESE-trending faults showing dextral movements (Fig. 8b). Based on the field data, we cannot determine if the thrusts are active structures or were active during the prolonged contractional history of this locality, which started at ~17 Ma (Silvestro and Atencio, 2009). Strike-slip structures, in contrast, affect Pliocene volcanic units, so we interpret them as active faults.

5. Kinematic analysis

Kinematic analysis of fault slip data was carried out on stations in all study areas (Figs. 3, 5, 6 and 8), and allowed us to characterize the movement of the mapped active faults.

Thrusts show pure dip-slip with a consistent E-W contraction direction. The P and T axes for each station are grouped in clusters indicating a well-defined contraction direction for this deformation. While some of the strike-slip faults affect Quaternary deposits (Fig. 5a), most kinematic data from strike-slip faults were measured on structures that affect Cretaceous rocks. In order to analyze the possibility that these structures were ancient faults previous to folding in the region, we compared the kinematic results in the deformed (current) and unfolded state (Fig. 9). In the deformed state, all strike-slip kinematic data indicate NW or E-W contraction directions, with some dispersion of P and T axes in spite of which the fields of contraction and extension are well defined (Fig. 9). In contrast, the unfolded data show different deformations: for stations with shallow dipping strata (both stations at Cajón de los Caballos and station 42 at Cerro Mollar, locations in Figs. 6 and 8), the

restoration does not change the kinematics of the faults. For stations with steeply dipping strata (stations 26 and 35 at Cerro Mollar and stations 9 and 16 at Cerro Pencal, locations in Figs. 3 and 6), the restored data indicate extension with NW to N extension directions.

We consider that the faults post-date folding because (i) the dependence of fault kinematics in the restored state on the current bedding dip (strike-slip for low dips and extension for high dips) suggests that the faults post-date folding; (ii) there are no indications of N-S extension between the Late Cretaceous and the Miocene in the region, and (iii) it seems unlikely that pre-folding faults with different kinematics and from different locations would be folded in such a way to produce kinematics consistent with a younger strike-slip deformation event recorded in the same localities.

We propose that both kinds of structures: N-trending thrusts and ESE- and WNW-trending strike-slip faults, were active during the Pliocene?-Quaternary to the present.

6. Stress state

6.a. Stress directions

We obtained principal stress axes directions from two independent sources: (i) maximum and minimum horizontal stress directions (S_{Hmax} and S_{hmin}) were measured from borehole breakouts in oil wells from the northern area; and (ii) the inversion of fault kinematic data (Angelier, 1975, 1984, 1990) which provides the direction of the three main stress axes and the stress ratio ϕ (see section 3. Methods).

Borehole breakouts were measured in three wells in the northern part of the study area (Cerro Pencal; Fig. 2). While the quality of breakout data was low due to the short length of the analyzed well sections (class D in the classification of the World Stress Map project; Sperner *et al.*, 2003; see Table 1), the results are consistent with regional studies (Guzmán *et al.*, 2007, 2011; Guzmán and

Cristallini, 2008) and those from inversion of fault kinematic data presented in this work, indicating E-W to ENE S_{Hmax} directions (Fig. 10).

Inversion of kinematic data for stress was carried out for three locations in Cerro Mollar, where we had the highest number of measurements. The results are shown in Figure 11 and Table 2. Stress directions are consistent with the kinematic P and T axes and with S_{Hmax} and S_{hmin} directions derived from borehole breakouts (Fig. 10). In addition to this, the stress ratio ϕ indicates similar magnitudes of σ_2 and σ_3 in one case (station 26, Table 2), while data from station 42 indicate a pure strike-slip regime and stations 35 and 36 indicate a pure reverse stress state.

6.b. Stress magnitudes

In order to better understand the stress state, we used wellbore data combined with geomechanical considerations to obtain the magnitude of stresses (see section 3. Methods). We calculated the vertical stress (σ_v) as a function of depth by integrating density data from wellbore profiling. The minimum principal stress magnitude was obtained from a mini-frac test (Zoback, 2010) carried out in a wellbore in the northern sector (Puesto Rojas) for a depth of 1277 m: σ_3=26 MPa (Fig. 12). At this same depth, the vertical stress from density data was σ_v=30.5 MPa.

Estimating the maximum stress σ_1 requires some assumptions. In our case study, since we know that there are active faults in the area, and assuming μ_s= 0.6 (see section 3.Methods), we obtain σ_1=80.6 MPa.

These results determine a stress state in which:

$\sigma_3 = 26$ MPa $< \sigma_2 = \sigma_v = 30.5$ MPa $< \sigma_1 = 80.6$ MPa

and therefore $\sigma_3 \sim \sigma_2 << \sigma_1$.

This stress regime corresponds to a reverse/strike-slip faulting environment in which both kinds of structures are active due to small fluctuations in the values of σ_3 and σ_2 that interchange the orientation of the minimum and intermediate stresses (Zoback, 2010).

The determined stress magnitudes and the differential stress ($\sigma_1 - \sigma_3 = 54.6$ MPa) are consistent with estimations from frontal regions of other orogens (Lacombe, 2001; Beaudoin and Lacombe, 2018).

7. Slip tendency analysis

Combining the results of sections 4 and 5, we carried out a slip tendency analysis (Morris *et al.*, 1996). As in the previous case, we assume $\mu_s = 0.6$, which implies that we are not considering weak faults that may be inherited from the pre-Andean history. We analyzed two cases, corresponding to the two alternating stress states that we propose for the region.

In the reverse faulting regime, $\sigma_3 = \sigma_v = 26$ MPa; $\sigma_1 = 80.6$ MPa is horizontal with a direction parallel to the Nazca-South America convergence (N80ºE), based on breakout data and the stress inversion for stations 35 and 36 (Fig. 11); and $\sigma_2 = 30.5$ MPa is horizontal and orthogonal to σ_1. In this stress state, N to NNW low-angle faults are active, consistent with the thrusts and backthrusts observed in the field (Fig. 13a,c).

In the strike-slip regime, σ_3 and σ_2 are interchanged, and therefore $\sigma_2 = \sigma_v = 30.5$ MPa and $\sigma_3 = 26$ MPa is horizontal and orthogonal to σ_1 that remains in the same orientation and magnitude of the previous case as obtained in station 26. This stress state activates high angle WNW and ENE strike-slip faults, like the ones mapped in the field (Fig. 13b,d). The same stress magnitudes but with a ESE-trending σ_1, like the one obtained for station 42 (Fig. 11) activate NW trending faults.

This indicates that the Pliocene to recent activity of N-trending thrusts and WNW- and ESE-strike slip faults can be the result of a reverse/strike-slip faulting regime in the region. In addition to this, pre-existing faults with those orientations will likely be reactivated.

8. Coulomb stress variations

We calculated the static stress changes in the faults of Cerro Pencal, Puesto Rojas and Cerro Mollar produced by the reverse faults mapped in the region, the Sosneado and Malargüe faults (Figs. 1 and 7), and the structures reported in this work. In particular, we analyzed the stress change on the strike-slip faults. With the Sosneado thrust or the Cerro Pencal and Puesto Rojas backthrusts as sources, static stress changes were not favorable to reactivation of the strike-slip faults. In contrast, the static stress change produced by a M=6 earthquake on the Malargüe fault produced positive and important values (higher than 0.3 MPa) on the strike-slip faults (Fig. 14). The highest values of static stress change on the studied faults are in dextral faults on the edges of the Malargüe fault, while values for the sinistral faults are also positive. This result suggests that seismic activity on the Malargüe fault favors seismicity on the strike-slip faults in the context of a reverse/strike-slip faulting regime (in the sense of Zoback, 2010).

9. Discussion

9.a. Tectonic implications

The stress field in the Andean retroarc is determined by a combination of the convergence of the Nazca and South American plates and topographic forces (Guzmán *et al.*, 2007): the general E-W trend of $S_H=\sigma_1$ is a response to the convergence direction, while topographic forces produce small rotations to ESE and WNW trends. Local deformation structures produce localized NNE to NNW trends (Guzmán *et al.*, 2007). Our results are consistent with the determinations of the orientation of S_H made by these authors in the frontal Malargüe fold-and-thrust belt.

The identification of active thrusts and strike-slip faults throughout the orogenic front of the Malargüe fold-and-thrust belt, and the relationship of these structures with the stress field, indicates that this region was not affected by an extensional collapse during the Pliocene-Quaternary as previously proposed by Ramos and Kay (2006) and Folguera *et al.* (2008, 2009). In contrast to this proposal, thrusts are active along parts of the orogenic front, indicating that the region is currently under compression.

The thrusts along the frontal Malargüe fold-and-thrust belt developed in the middle Miocene (~15 Ma, Silvestro *et al.*, 2005) and were episodically active since that time, accumulating significant displacement (more than 3 km according to Giambiagi *et al.*, 2009b). The thrusts are cross-cut by oblique strike-slip faults with tens of meters of displacement which postdate folding in thrust-related anticlines, and were likely active since the Pliocene-Quaternary.

The stress state determined from inversion of fault slip data and available well bore information (minifrac test) corresponds to a reverse/strike-slip faulting regime (Zoback, 2010) in which σ_2 and σ_3 have similar magnitudes and are locally exchanged, which leads to an alternation of the activity of both kinds of structures producing the "σ_2 paradox" defined by Tavani *et al.* (2015). Furthermore, a Coulomb static stress change analysis indicates that in this stress regime, activity on the basement N-trending reverse faults increases the likelihood of activation of the strike-slip faults. We therefore propose that strike-slip faults were active for short periods of time following earthquakes on the major reverse faults.

A model of the evolution of the region during the Miocene (Barrionuevo *et al.*, under review) suggests that these variations in the stress regime are a long-term feature of the orogenic front and that the alternation between compression and strike-slip deformation took place intermittently in different sectors of the Malargüe area during the Neogene and Quaternary.

9.b. Implications for seismic hazard

The study area is located ~25 km away from the main city in southernmost Mendoza province, Malargüe, that has a population of over 26.000 according to the 2010 census. Important infrastructure related to oil extraction activities is found within the study area and its surroundings.

While there is no record of destructive local earthquakes in the study area, probably due to the recent permanent population of the region (the city of Malargüe was founded in 1886), low-magnitude seismic activity has been detected in the region (Fig. 1). Instrumental seismicity is restricted to international or national networks (PDE and INPRES catalogs) and local seismic experiments located near the region (Spagnotto *et al.*, 2015). All the events with depths lower than 20 km have magnitudes $M \leq 4.5$. Important activity has been observed in the Sosneado thrust (Fig. 1), already documented as an active structure by Giambiagi *et al.* (2008). Only a few events have been detected in the study area and can be the result of activity either on the Malargüe and Puchenque faults or on the oblique strike-slip faults.

In order to estimate the implications of the main active faults recognized in this work for seismic hazard, we determined the maximum possible earthquake magnitude for the thrusts from their surface length, based on the equations available in the literature (Wells and Coppersmith, 1994; Wesnousky, 2008; Leonard, 2010). We calculated the maximum moment magnitude (M_w) for the Cerro Pencal backthrust and the Puesto Rojas backthrust as separate structures, and also combined in case both can rupture as a single fault. The result shows potential M_w between 5.5 and 6.2 (Table 3), which suggests that these faults can generate moderate earthquakes that should be taken into account in seismic hazard and risk studies.

10. Conclusions

We document active orogen parallel thrusts and oblique strike-slip faults in the orogenic front of the

Malargüe fold-and-thrust belt, in the Andes between 35° and 36°S. Based on the available data, we propose that the Pliocene and Quaternary activity of both kinds of faults is the result of a reverse/strike-slip faulting regime in which $\sigma_3 \sim \sigma_2 << \sigma_1$. The lack of historical destructive earthquakes in the region is likely a reflection of the recent permanent population of the area and the long recurrence period of the structures, however, based on their surface length, we estimate that the thrusts can produce earthquakes of magnitude ~6.

Acknowledgements

We thank reviewers Adolph Yonkee and Víctor Ramos, and special issue editors Pablo Granado and Olivier Lacombe for constructive comments that helped us to improve the paper. We thank Midland Valley Ltd.for a 2018 academic license of their software Move. Funding was provided by Agencia Nacional de Promoción Científica y Técnica grant PICT2015-1181 to JFM.

References

Allmendinger, R. W. (2001), FaultKinWinFull version 1.2.2. A program for analyzing fault slip data for Windows™ computers. [Available at http://www.geo.cornell. edu/ geology/faculty/RWA/programs.html, last accessed 19/4/2019]

Anderson, E.M., 1951. The Dynamics of Faulting. Oliver and Boyd, Edinburgh.

Angelier, J., 1975. Sur l'analyse de mesures recueillies dans des sites faillés : l'utilité d'une confrontation entre les méthodes dynamiques et cinématiques. C. R. Acad. Sci. Paris, Ser. D 281, 1805–1808.

Angelier, J., 1984. Tectonic analysis of fault slip data sets. J. Geophys. Res. 89 (B7), 5835–5848.

Angelier, J., 1990. Inversion of field data in fault tectonics to obtain the regional stress. III: a new

rapid direct inversion method by analytical means. Geophys. J. Int. 103, 363–376.

Baldauf, P.E., 1997. Timing of the uplift of the Cordillera Principal, Mendoza Province, Argentina [Ph.D. thesis]: Washington, D.C., George Washington University, 356 p.

Beaudoin, N., Lacombe, O., 2018. Recent and future trends in paleopiezometry in the diagenetic domain: Insights into the tectonic paleostress and burial depth history of fold-and-thrust belts and sedimentary basins. Journal of Structural Geology, 114: 357-365.

Bell, J.S., Gough D.I., 1982. The use of borehole breakouts in the study of crustal stress, U.S. Geol. Surv. Open File Rep., 82-1075, 539 – 557.

Boll, A., Alonso, J., Fuentes, F., Vergara, M., Laffitte, G., Villar, H., 2014. Factores controlantes de las acumulaciones de hidrocarburos en el sector norte de la Cuenca Neuquina, entre los ríos Diamante y Salado, provincia de Mendoza, Argentina. IX Congreso de Exploración y Desarrollo de Hidrocarburos, Actas: 3-44.

Byerlee, J. 1978. Friction of rocks. Pure and Applied Geophysics 116, 615–26.

Cegarra M.I., Ramos V.A. (1996) La faja plegada y corrida del Aconcagua. In Ramos VA (ed) Geología de la región del Aconcagua, provincias de San Juan y Mendoza. Subsecretaría de Minería de la Nación, Dirección Nacional del Servicio Geológico, Anales 24:387-422.

Chapple,W.M., 1978. Mechanics of thin-skinned fold-and-thrust belts. Geol. Soc. Am. Bull. 89 (8), 1189–1198.Charrier R, Pinto L, Rodríguez MP (2007) Tectonostratigraphic evolution of the Andean orogen in

Chile. In Moreno T,, Gibbons W (eds) The Geology of Chile. The Geological Society: 21-114.

Cox, J.W. (1970), The high resolution dipmeter reveals dip – related borehole and formation characteristics, Trans. SPWLA Annu. Logging Symp., 11, 3–6.

Elliott, D., 1976. The motion of thrust sheets. J. Geophys. Res. 81 (5), 949–963.

Folguera, A., Bottessi, G., Zapata, T., Ramos, V.A., 2008. Crustal collapse in the Andean backarc

since 2 Ma: Tromen volcanic plateau, Southern Central Andes (36°40′-37°30′S). Tectonophysics, 459: 140-160.

Folguera, A., Naranjo, J., Orihashi, Y., Sumino, H., Nagao, K., Polanco, E., Ramos, V.A., 2009. Retroarc volcanism in the northern San Rafael Block (34°–35°30′S), southern Central Andes: Occurrence, age, and tectonic setting. Journal of Volcanology and Geothermal Research, 186: 169-185.

Giambiagi, L.B., Bechis, F., García, V., and Clark, A., 2008, Temporal and spatial relationship between thick- and thin-skinned deformation in the Malargüe fold and thrust belt, southern Central Andes: Tectonophysics, v. 459, p. 123–139, doi: 10 .1016 /j .tecto .2007 .11 .069

Giambiagi LB, Tunik M, Barredo S, Bechis F, Ghiglione M, Alvarez P, Drosina M (2009a). Cinemática de apertura del sector norte de la cuenca Neuquina. Revista de la Asociación Geológica Argentina 65(2):278-292.

Giambiagi, L., Ghiglione, M., Cristallini, E., and Bottesi, G., 2009b. Kinematic models of basement/cover interactions: Insights from the Malargüe fold and thrust belt, Mendoza, Argentina: Journal of Structural Geology, v. 31, p. 1443–1457, doi: 10.1016/j.jsg.2009.10.006.

Giambiagi, L.B., Mescua, J.F., Bechis, F., Tassara, A., Hoke, G., 2012. Thrust belts of the Southern Central Andes: along strike variations in shortening, topography, crustal geometry and denudation. GSA Bulletin, 124 (7-8): 1339-1351. doi:10.1130/B30609.1

Giambiagi, L., Alvarez, P., Spagnotto, S., 2015. Temporal variation of the stress field during the construction of the central Andes: Constrains from the volcanic arc region (22–26°S), Western Cordillera, Chile, during the last 20 Ma., 2016. Tectonics, 35 (9): 2014-2033.

Guzmán, C., Cristallini, E., Bottesi, G., 2007. Contemporary stress orientations in the Andean retroarc between 34S and 39S from borehole breakout analysis, Tectonics, 26, TC3016, doi:10.1029/2006TC001958

Guzmán, C., Cristallini, E., 2009. Contemporary stress orientations from borehole breakout

analysis in the southernmost flat-slab boundary Andean retroarc (32º44´ and 33º 40´S).

Journal of Geophysical Research 114 (B2):B02406. doi: 10.1029/2007JB005505.

Guzmán, C., Cristallini, E., García, V., Yagupsky, D., Bechis, F., 2011. Evolución del campo de esfuerzos horizontal desde el Eoceno a la actualidad en la Cuenca Neuquina. Revista de la Asociación Geológica Argentina 68 (4): 542 - 554.

Hernando, I., Franzese, J., Llambías, E.J., Petrinovic, I.A., 2014. Vent distribution in the Quaternary Payún Matrú Volcanic Field, western Argentina: Its relation to tectonics and crustal structures. Tectonophysics, 622: 122–134.

Horton, B., Fuentes, F., Boll, A., Starck, D., Ramírez, S., Stockli, D., 2016. Andean stratigraphic record of the transition from backarc extension to orogenic shortening: A case study from the northern Neuquén Basin, Argentina. Journal of South American Earth Sciences, 71: 17-40.

Jaeger, J.C., Cook, N., 1979. Fundamentals of Rock Mechanics. London: Chapman and Hall, 593 pp.

King, G., Stein, R., Lin, J., 1994. Static stress changes and the triggering of earthquakes. Bulletin of the Seismological Society of America, 84(3): 935-953.

Kozlowski, E., Manceda, R., and Ramos, V.A., 1993, Estructura, in Ramos, V.A., ed., Geología y Recursos Naturales de Mendoza: 12 Congreso Geológico Argentino y 2 Congreso de Exploración de Hidrocarburos, Relatorio, p. 235–256.

Lacombe, O., 2001. Paleostress magnitudes associated with development of mountain belts: insights from tectonics analyses of calcite twins in the Taiwan foothills. Tectonics, 20(6): 834-849.

Lacombe, O., 2012. Do fault slip data inversions actually yield ‘‘paleostresses’’ that can be compared with contemporary stresses? A critical discussion. Comptes Rendus Geoscience, 344: 159-173.

Leanza, H.A. 2003. Las sedimentitas huitrinianas y rayosianas (Cretácico inferior) en el ámbito central y meridional de la cuenca Neuquina, Argentina. Servicio Geológico y Minero Argentino,

Serie Contribuciones Técnicas, Geología, 2:1-31

Legarreta, L. and Gulisano, C.A., 1989. Análisis estratigráfico secuencial de la cuenca Neuquina (Triásico superior- Terciario inferior). In G. Chebli y L. Spalletti (eds.), Cuencas Sedimentarias Argentinas. Facultad de Ciencias Naturales, Universidad Nacional de Tucumán, Correlación Geológica Serie 6: 221-243, Tucumán.

Legarreta, L., and Uliana, M.A., 1999, El Jurásico y Cretácico de la Cordillera Principal y la cuenca Neuquina. 1. Facies sedimentarias, in Caminos, R., ed., Geología Argentina: Servicio Geológico y Minero Argentino, Instituto de Geología y Recursos Minerales, Anales, v. 29, p. 399–416.

Llambías, E.J., Kleiman, L.E., and Salvarredi, J.A., 1993, El magmatismo gondwánico, in Ramos, V.A., ed., Geología y Recursos Naturales de Mendoza: 12 Congreso Geológico Argentino y 2 Congreso de Exploración de Hidrocarburos, Relatorio, p. 53–64.

Manceda, R., and Figueroa, D., 1995, Inversion of the Mesozoic Neuquen rift in the Malargüe fold-thrust belt, Mendoza, Argentina, in Tankard, A.J., et al., eds., Petroleum basins of South America: American Association of Petroleum Geologists Memoir 62, p. 369–382.

Mescua, J.F., Giambiagi, L.B., Bechis, F., 2008. Evidencias de tectónica extensional en el Jurásico tardío (Kimeridgiano) del suroeste de la provincia de Mendoza. Revista de la Asociación Geológica Argentina, 63(4): 512-519.

Mescua, J.F., Giambiagi, L.B., Tassara, A., Giménez, M., Ramos, V.A., 2014. Influence of pre-Andean history over Cenozoic foreland deformation: Structural styles in the Malargüe fold-and-thrust belt at 35ºS, Andes of Argentina. Geosphere, 10(3): 585-609.

Mpodozis, C. and Ramos, V.A., 1989. The Andes of Chile and Argentina. In Ericksen, G.E., Cañas Pinochet, M.T. y Reinemud, J.A. (eds.), Geology of the Andes and its relation to hydrocarbon and mineral resources. Circumpacific Council for Energy and Mineral Resources, Earth Sciences Series, 11: 59-90.

Morris, A., Ferrill, D., Brent Henderson, D., 1996. Slip tendency analysis and fault reactivation.

Geology, 24: 275-278.

Ramos, V.A., and Kay, S.M., 2006, Overview of the tectonic evolution of the southern Central Andes of Mendoza and Neuquén (35°-39°S latitude), in Kay, S.M., and Ramos,

V.A., eds., Evolution of an Andean margin: A tectonic and magmatic view from the Andes to the Neuquén Basin (35°–39°S lat), Geological Society of America Special Paper 407, p. 1–18, doi: 10.1130/2006.2407(01).

Rojas, L., Radic, J.P., 2002. Estilos de deformación del basamento y de la cobertura sedimentaria en la faja plegada y fallada de Malargüe en el área de Puesto Rojas, Mendoza, Argentina. 15° Congreso Geológico Argentino, Actas 2: 224-229.

Silvestro, J., Kraemer, P., Achilli, F., Brinkworth, W., 2005, Evolución de las cuencas sinorogénicas de la Cordillera Principal entre 35°-36° S, Malargüe. Revista de la Asociación Geológica Argentina, v. 60, p. 627–643.

Silvestro, J., Atencio, M., 2009. La cuenca cenozoica del río Grande y Palauco: edad evolución y control estructural, faja plegada de Malargüe. Revista de la Asociación Geológica Argentina, 65(1): 154-169.

Spagnotto, Silvana; Triep, Enrique; Giambiagi, Laura; Lupari, Marianela 2015 Triggered seismicity in the andean arc region via static stress variation by the Mw=8.8, february 27, 2010, Maule earthquake. Journal of South American Earth Sciences. vol. 63 p. 36 - 47.

Sperner, B., Müller, B., Heidbach, O., Delvaux,D., Reinecker, J., Fuchs, K., 2003. Tectonic stress in the Earth's crust: Advances in the World Stress Map Project. In New Insights Into Structural Interpretation and Modeling, edited by D. Nieuwland, Geol. Soc. Spec. Publ., 212, 101 – 116.

Tavani, S., Storti, F., Lacombe, O., Corradetti, A., Muñoz, J.A., Mazzoli, S., 2015. A review of deformation pattern templates in foreland basin systems and fold-and-thrust belts: Implications for the state of stress in the frontal regions of thrust wedges. Earth Science Reviews, 141:82-104.

Tunik, M., Folguera, A., Naipauer, M., Pimentel, M. y Ramos, V.A., 2010. Early uplift and orogenic

deformation in the Neuquén basin: Constraints on the Andean uplift from U-Pb and Hf isotopic data of detrital zircons. Tectonophysics, 489: 258-273.

Yagupsky, D., Cristallini, E., Fantín, J., Zamora Valcarce, G., Botessi, G., and Varadé, R., 2008, Oblique half-graben inversion of the Mesozoic Neuquén rift in the Malargüe fold and thrust belt, Mendoza, Argentina: New insights from analogue models: Journal of Structural Geology, v. 30, p. 839–853, doi: 10 .1016 /j .jsg .2008 .03 .007 .

Zalohar, J., and M. Vrabec (2007), Paleostress analysis of heterogeneous fault-slip data: the Gauss method, J. Struct. Geol., 29, 1798–1810.

Zoback, M., 2010. Reservoir geomechanics. Cambridge University Press, 449 p. Cambridge.

Zoback, M., Townend, J., 2001. Implications of hydrostatic pore pressures and high crustal strength for the deformation of intraplate lithosphere. Tectonophysics, 336: 19-30.

Zoback, M., Moss, D.,Mastin, L.G., Anderson R.N., 1985. Well bore breakouts and in situ stress, J. Geophys. Res., 90, 5523 – 5530.

Figure captions

Figure 1. Location of the study area. (A) LANDSAT ETM+ image (RGB742 band combination) of the orogenic front of the Malargüe fold-and-thrust belt. White boxes correspond to the areas where active faults were recognized in this work. The dashed line is the approximate location of the Malargüe fold-and-thrust belt orogenic front. Red lines indicate the maximum horizontal stress (S_H) determined by Guzmán *et al.* (2007) based on borehole breakout determinations. Yellow dots are upper crustal seismic events (depth ≤ 20 km) from the INPRES catalog (1999-2018; www.inpres.gob.ar), PDE catalog (1953-2018; https://earthquake.usgs.gov/data/pde.php), and Spagnotto et al. (2015). All events have magnitudes lower than 4.5. (B) Geologic map based on Giambiagi et al. (2012).

Figure 2. (A) Location of northern study areas over LANDSAT ETM+ band 8, indicating the main active structures. Outcrops of Cretaceous to Pliocene rocks are shown, the rest of the study area is covered by Quaternary deposits. (B,C,D) Geologic maps for the northern study areas.

Figure 3. Active faults at Cerro Pencal, location in Fig. 2. (A, B) Cerro Pencal backthust which places Late Cretaceous redbeds over Quaternary deposits. (C) Mapped structures over Google Earth image, insets show kinematic data of minor faults indicating pure reverse movement of the Cerro Pencal backthrust and sinistral movement of the oblique strike-slip faults. The yellow dot indicates the location of Fig. 4. (D, E) Strike-slip fault zones consisting of small faults with metric displacement. Inset in (E) shows kinematic data for the strike-slip faults.

Figure 4. Minor east-verging thrust developed in Quaternary deposits at Cerro Pencal. Location in Figs. 2B and 5.

Figure 5. Active faults at Puesto Rojas, location in Fig. 2. (A) Strike-slip fault affecting mid-Cretaceous rocks and Quaternary deposits. (B) Thrust placing mid-Cretaceous limestones over Quaternary deposits. (C) Mapped structures over Google Earth image. Inset shows kinematic data for a reverse fault zone consisting of minor thrusts. (D, E) Minor faults with tens of cm of displacement associated with the thrust that uplifts Cretaceous rocks over Quaternary deposits.

Figure 6. Active faults at Cerro Mollar, location in Fig. 2. (A) Thrust placing Cretaceous redbeds over Quaternary deposits. (B) Thrust placing mid-Cretaceous limestones over Quaternary deposits. (C) Mapped structures over Google Earth image. Insets show kinematic data for reverse and sinistral faults. (D, E) Strike-slip faults on Late Cretaceous redbeds.

Figure 7. (A) Regional cross-section across the Malargüe fold-and-thrust belt from Giambiagi *et al.* (2012). Note how the displacement on basement faults such as the Puchenque and Malargüe faults is transferred to thin-skinned thrusts that reach the surface in the study area. (B, C) Cross-sections through the Puesto Rojas (B) and Cerro Mollar (C) sectors, showing the relationship between basement reverse faults and the active faults presented in this work, located with red arrows. Modified from Rojas and Radic (2002).

Figure 8. Active strike-slip faults in the Cajón de los Caballos, location in Fig. 2. (A) Geologic map of the Cajón de los Caballos area. (B) Mapped structures over Google Earth image. Insets show kinematic data for minor faults associated with two of the strike-slip faults.

Figure 9. Kinematic fault-slip data for strike slip faults. For each station, the left stereonet shows the measured data and the right stereonet shows the data after bed unfolding. Note that all the

measured data correspond to a compatible deformation with roughly E-W contraction, while the unfolded data produce different deformations depending on bedding dip at each stations, which indicates that the measured faults post-date the folding.

Figure 10. Maximum (S_H) and minimum (S_h) horizontal stress derived from borehole breakout data.

Figure 11. Stress inversion results. The direction of σ_1 is shown in red arrows and the direction of σ_3 in blue arrows. Location of stations in Fig. 6

Figure 12. Mini-frac test in a well of the Puesto Rojas area. The Fracture Propagation Pressure corresponds to the minimum principal stress magnitude (3774 psi=26 MPa).

Figure 13. Results of slip tendency analysis. Colors indicate slip tendency value for fault plane poles. Faults with slip tendency>0.6 are active in the proposed stress field. (A) Reverse faulting regime with σ_1 of azimuth 80º. (B) Strike-slip faulting regime with σ_1 of azimuth 80º. (C) Thrust planes mapped in the study area, color coded to show their slip tendency in the compressional stress field. Note that high-angle reverse faults show low slip tendency (green color) suggesting that some mechanism has to act to produce their movement (e.g., high fluid pressure). Low angle reverse faults show high slip tendency (yellow color). (D) Strike-slip faults mapped in the study area, color coded to show their slip tendency in the strike-slip stress field. Sinistral, WNW faults show the highest slip tendency (red color). Dextral ESE faults also show high slip tendency (yellow), whereas sinistral NW faults show low slip tendency (green color). However these sinistral NW faults fall in the red field if σ_1 has an azimuth of 110º, also observed in the study area.

Figure 14. Coulomb static stress change. In all cases the source is a M_w=6 earthquake on the Malargüe fault and the receptors are: (A) dextral faults (strike 67.5°, vertical), (B) sinistral faults (strike 112.5°, vertical), and (C) reverse faults (strike 0°, dip 30°).

Table 1. Borehole breakout data from the Cerro Pencal sector.

Wellbore A

Unit	Length (m)	S_H strike	Quality
Avilé Member	40	78	D
Lower Agrio Formation	200	66	

Wellbore B

Unit	Length (m)	S_H strike	Quality
Avilé Member	82	88	D
Lower Agrio Formation	50	82	

Wellbore C

Unit	Length (m)	S_H strike	Quality
Avilé Member	44	97	D

Table 2. Stress inversion of kinematic data. n= number of measurements used for the inversion; nT= total number of measurements; $\sigma_1,\sigma_2,\sigma_3$= principal stress axes; $\phi=(\sigma2-\sigma3)/(\sigma1-\sigma3)$; and α=misfit angle. Stress regimes are: SL/R=strike-slip/reverse; R/SL= reverse/strike-slip; SL=strike-slip.

Site	Latitude	Longitude	n	nT	σ_1	σ_2	σ_3	ϕ	α	Regime
26	35°17’47,54’’S	69°48’02,33’’W	12	12	44/13	288/63	140/23	0,10	14	SL/R
35	35°19’48,84’’S	69°42’03,17’’W	18	20	272/2	3/25	178/64	0,60	27	R
36	35°19’45,31’’S	69°41’55,22’’W	16	16	277/0	187/2	21/88	0,69	20	R
42	35°19’42,02’’S	69°42’56,51’’W	21	25	248/2	358/84	158/6	0,50	17	SL

Table 3. Maximum earthquake magnitude estimated from the surface length of thrusts in the study area.

Fault	Surface length (m)	Maximum magnitude Wells and Coppersmith (1994)	Maximum magnitude Wesnousky (2008)	Maximum magnitude Leonard (2010)
Cerro Pencal backthust	5500	5.8	5.5	5.8
Puesto Rojas backthrust	7000	5.9	5.7	5.9
Cerro Pencal + Puesto Rojas backthrust	12500	6.2	6.2	6.2

Highlights

* We document active orogen parallel reverse faults and oblique strike-slip faults in the orogenic front of the Andes between 35° and 36°S

* A strike-slip/reverse faulting regime in which the minimum and intermediate principal stresses are similar in magnitude is deduced from the inversion of fault kinematic data and a mini-frac test

* Based on surface length, the active thrusts can produce seismic activity with magnitudes ~6

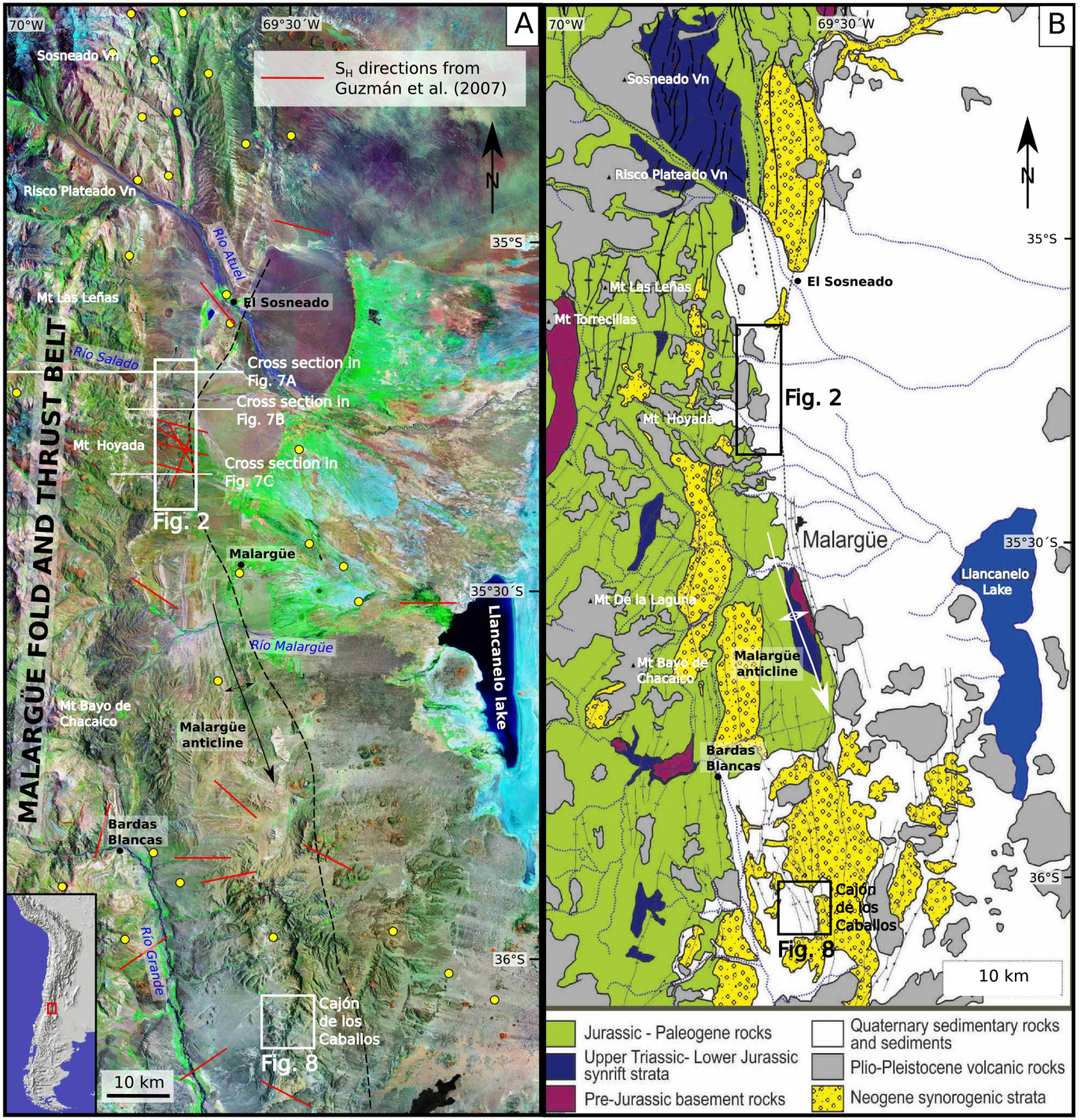
A
B
70°W
69°30´W
S_H directions from Guzmán et al. (2007)
N
Sosneado Vn
Risco Plateado Vn
Río Atuel
35°S
Mt Las Leñas
El Sosneado
Río Salado
Cross section in Fig. 7A
Cross section in Fig. 7B
Cross section in Fig. 7C
Mt Hoyada
Fig. 2
MALARGÜE FOLD AND THRUST BELT
Malargüe
35°30´S
Llancanelo lake
Río Malargüe
Mt Bayo de Chacaico
Malargüe anticline
Bardas Blancas
Río Grande
Cajón de los Caballos
Fig. 8
36°S
10 km
Mt Torrecillas
Mt De la Laguna
Llancanelo Lake
Jurassic - Paleogene rocks
Upper Triassic- Lower Jurassic synrift strata
Pre-Jurassic basement rocks
Quaternary sedimentary rocks and sediments
Plio-Pleistocene volcanic rocks
Neogene synorogenic strata

Figure 1

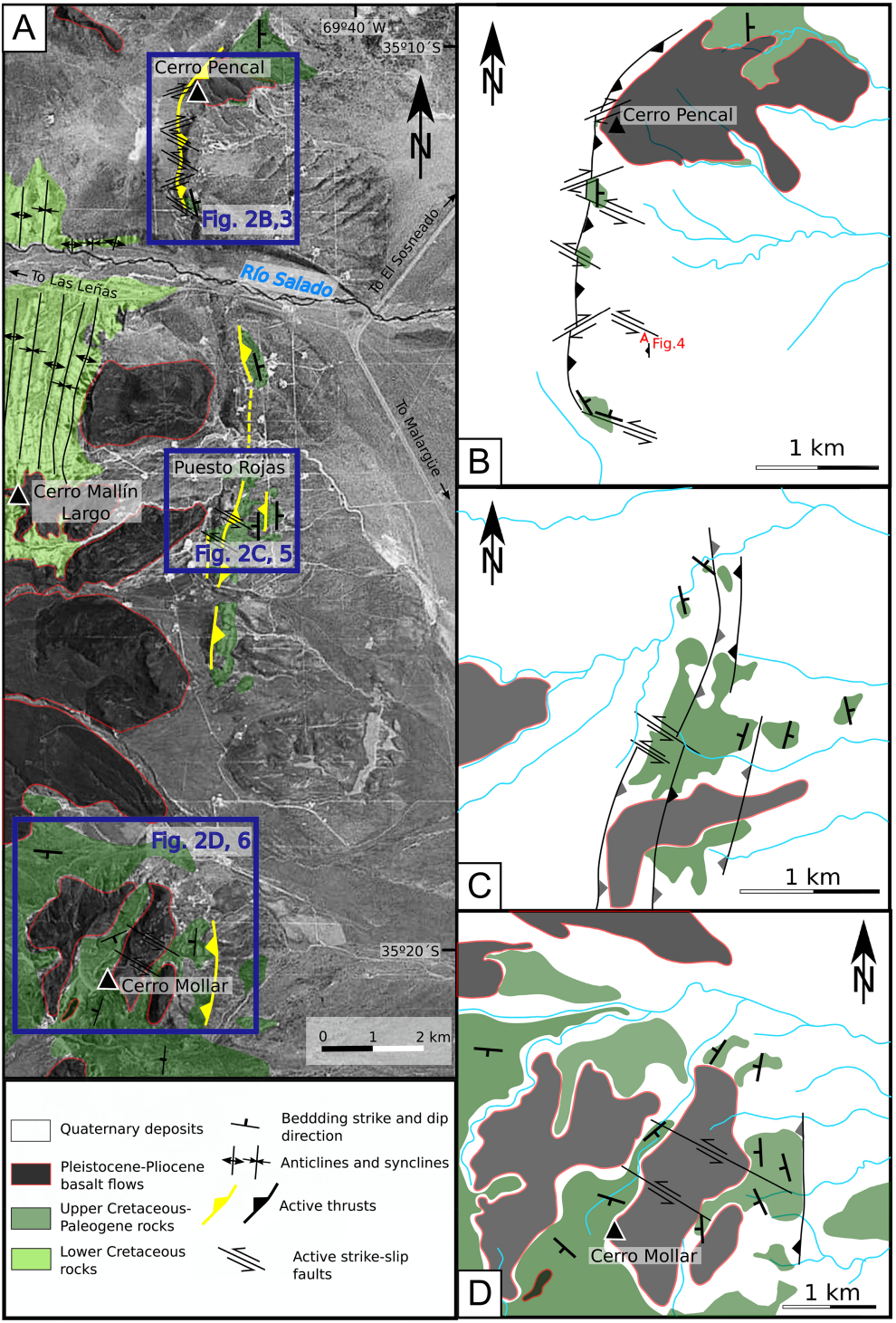
A
69º40´W
35º10´S
Cerro Pencal
Fig. 2B,3
N
To El Sosneado
Río Salado
To Las Leñas
To Malargüe
Puesto Rojas
Cerro Mallín Largo
Fig. 2C, 5
Fig. 2D, 6
35º20´S
Cerro Mollar
0 1 2 km
Quaternary deposits
Pleistocene-Pliocene basalt flows
Upper Cretaceous-Paleogene rocks
Lower Cretaceous rocks
Beddding strike and dip direction
Anticlines and synclines
Active thrusts
Active strike-slip faults
B
Cerro Pencal
A
Fig.4
1 km
C
1 km
D
Cerro Mollar
1 km

Figure 2

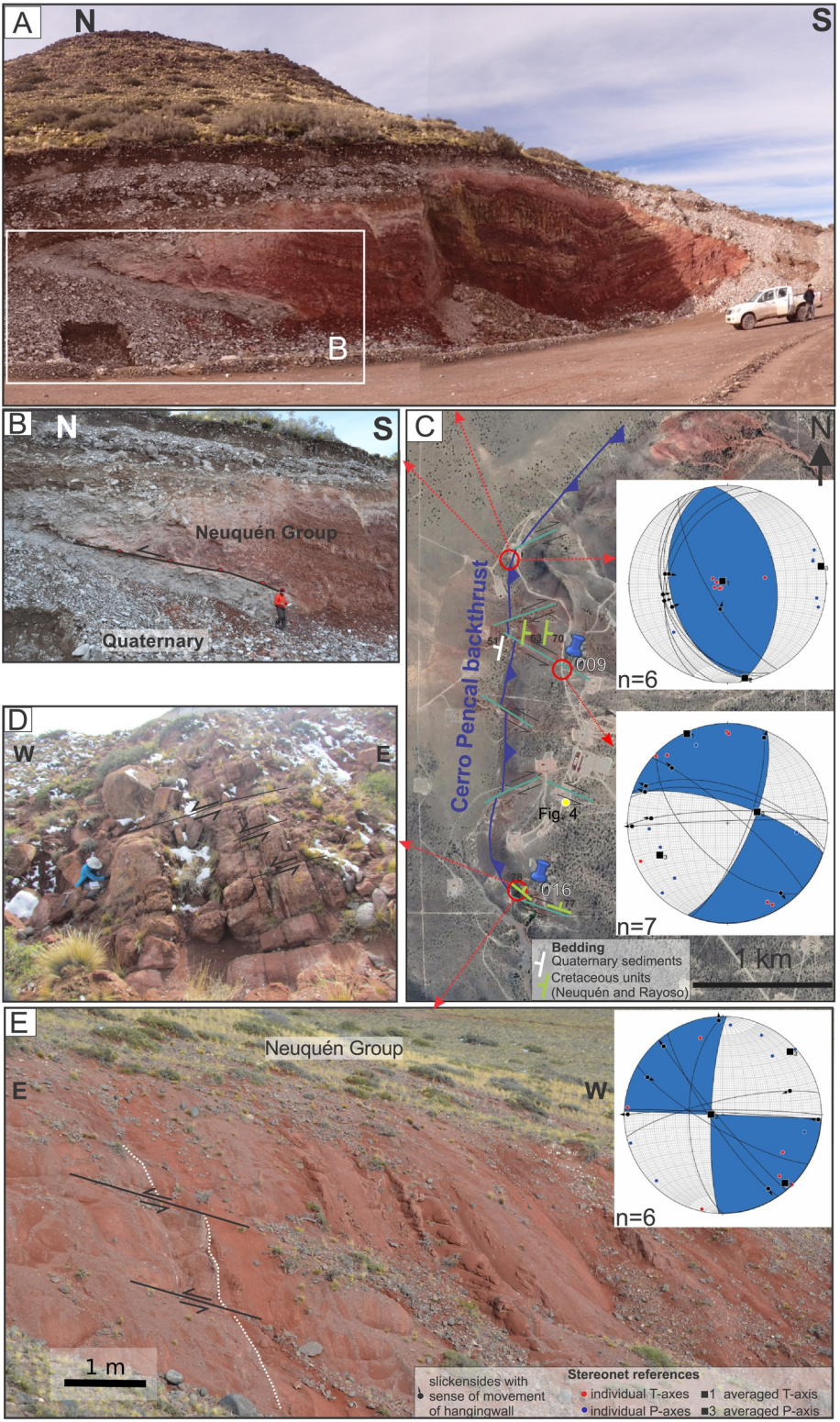
A
N
S
B
B
N
S
Neuquén Group
Quaternary
C
N
Cerro Pencal backthrust
009
016
Fig. 4
n=6
n=7
Bedding
Quaternary sediments
Cretaceous units
(Neuquén and Rayoso)
1 km
D
W
E
E
Neuquén Group
E
W
n=6
1 m
slickensides with
sense of movement
of hangingwall
Stereonet references
individual T-axes
averaged T-axis
individual P-axes
averaged P-axis

Figure 3

Figure 4

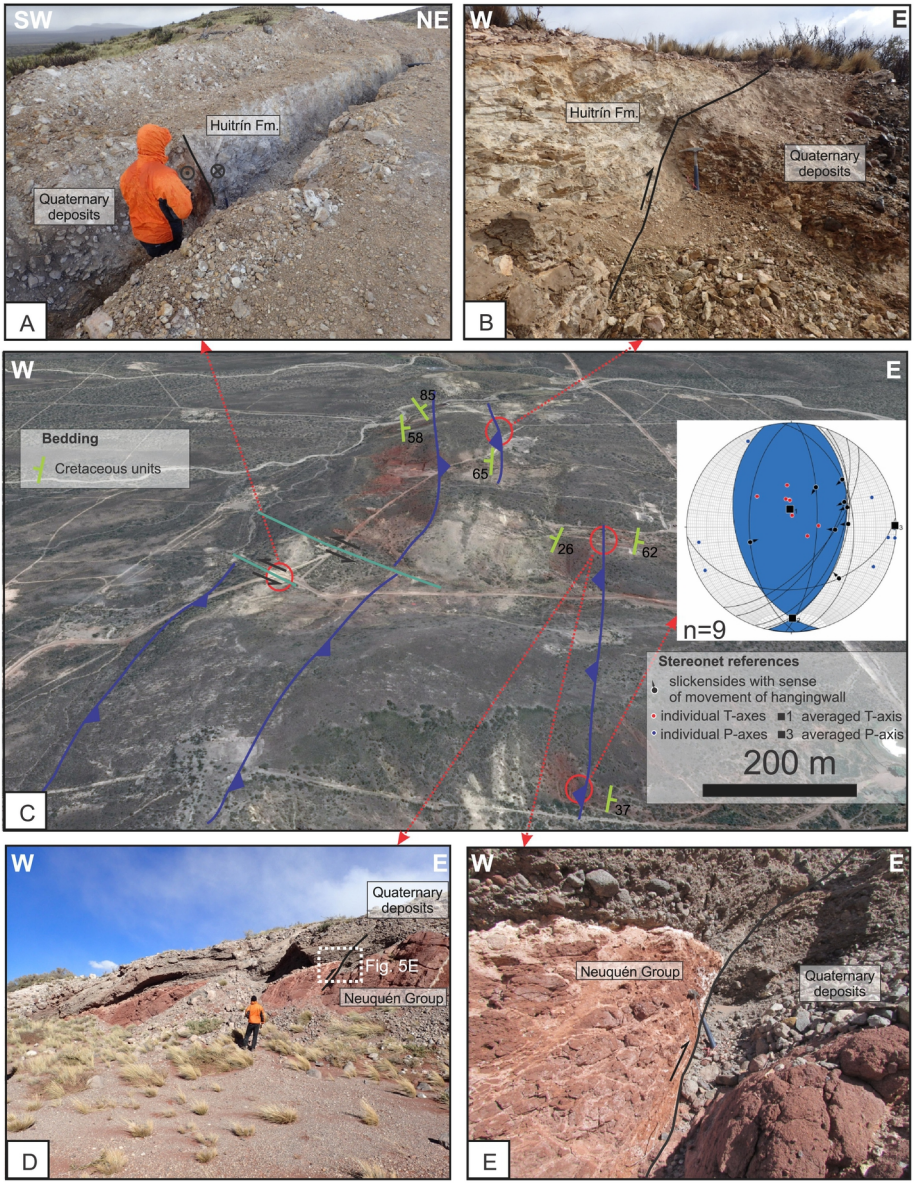
SW
NE
Huitrín Fm.
Quaternary deposits
A
W
E
Huitrín Fm.
Quaternary deposits
B
W
E
Bedding
Cretaceous units
85
58
65
26
62
37
n=9
Stereonet references
slickensides with sense of movement of hangingwall
individual T-axes
1 averaged T-axis
individual P-axes
3 averaged P-axis
200 m
C
W
E
Quaternary deposits
Fig. 5E
Neuquén Group
D
W
E
Neuquén Group
Quaternary deposits
E

Figure 5

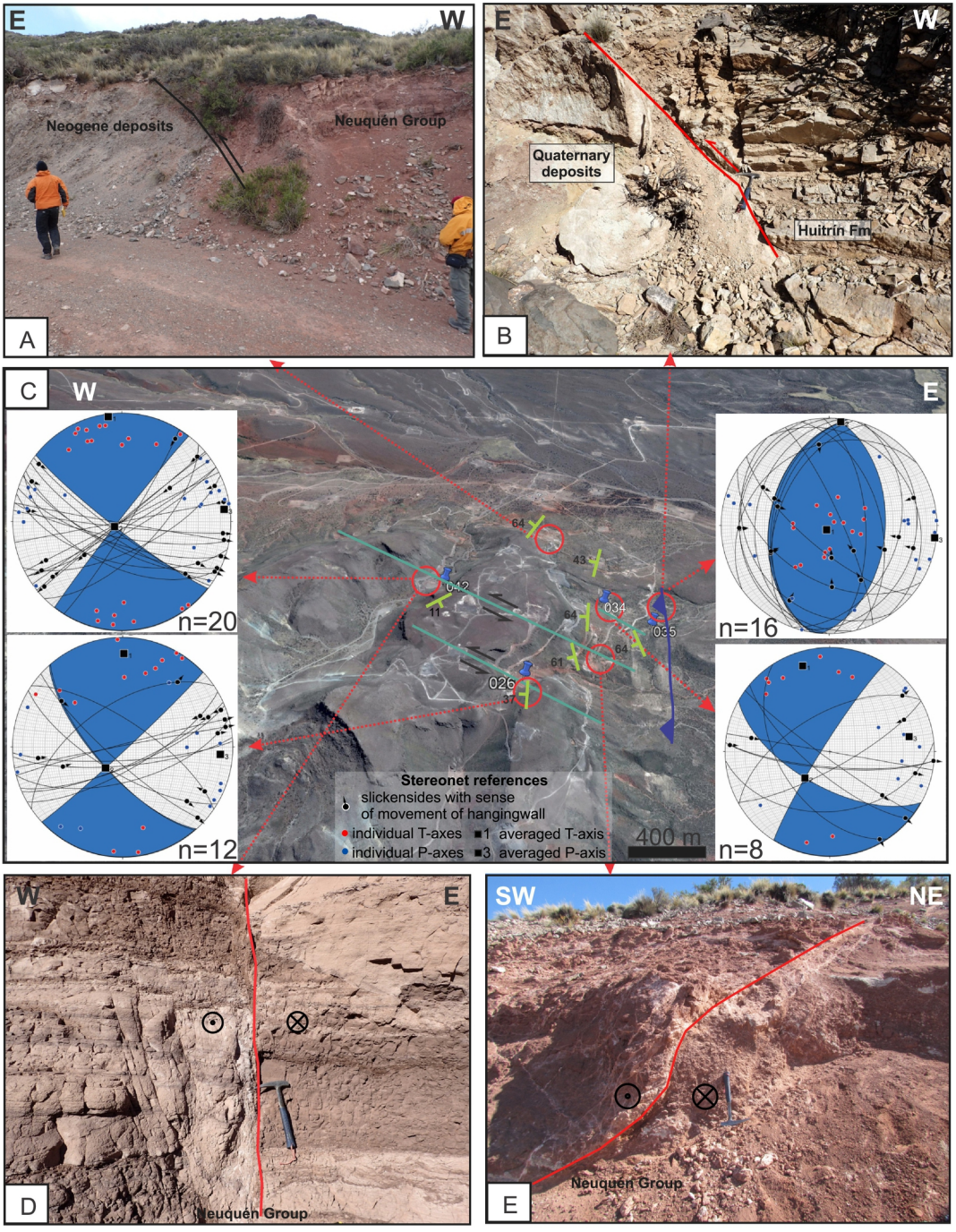
E
W
Neogene deposits
Neuquén Group
A
E
W
Quaternary deposits
Huitrín Fm
B
C
W
E
n=20
n=12
n=16
n=8
64
43
042
11
64
034
035
64
61
026
37
Stereonet references
slickensides with sense of movement of hangingwall
individual T-axes
1 averaged T-axis
individual P-axes
3 averaged P-axis
400 m
W
E
Neuquén Group
D
SW
NE
Neuquén Group
E

Figure 6

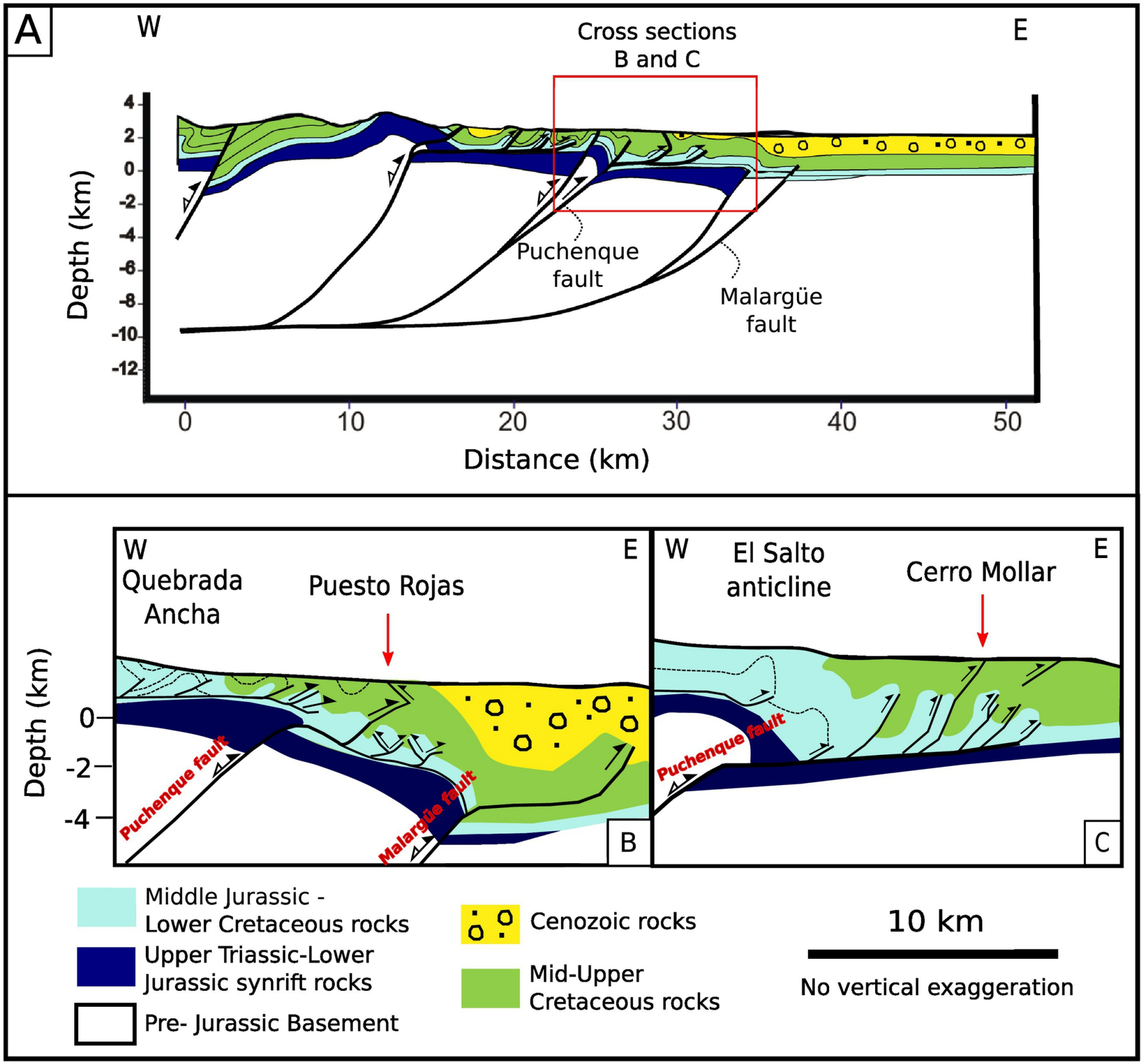
A
W
Cross sections
B and C
E
Depth (km)
4
2
0
-2
-4
-6
-8
-10
-12
Puchenque
fault
Malargüe
fault
0
10
20
30
40
50
Distance (km)
W
Quebrada
Ancha
Puesto Rojas
E
Depth (km)
0
-2
-4
Puchenque fault
Malargüe fault
B
W
El Salto
anticline
Cerro Mollar
E
Puchenque fault
C
Middle Jurassic -
Lower Cretaceous rocks
Upper Triassic-Lower
Jurassic synrift rocks
Pre- Jurassic Basement
Cenozoic rocks
Mid-Upper
Cretaceous rocks
10 km
No vertical exaggeration

Figure 7

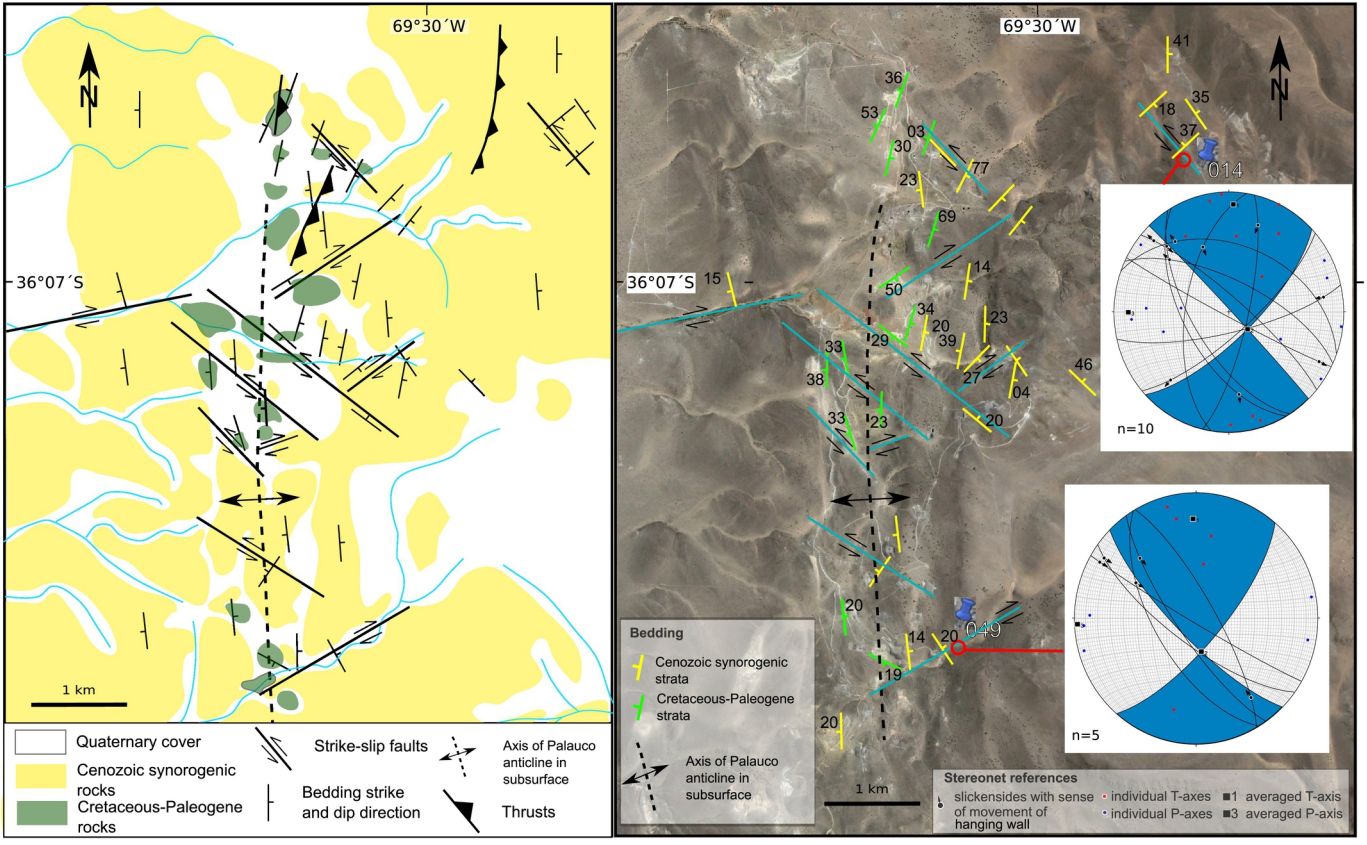
69°30´W
36°07´S
N
1 km
Quaternary cover
Cenozoic synorogenic rocks
Cretaceous-Paleogene rocks
Strike-slip faults
Bedding strike and dip direction
Axis of Palauco anticline in subsurface
Thrusts
Bedding
Cenozoic synorogenic strata
Cretaceous-Paleogene strata
Axis of Palauco anticline in subsurface
014
049
n=10
n=5
Stereonet references
slickensides with sense of movement of hanging wall
individual T-axes
individual P-axes
averaged T-axis
averaged P-axis

Figure 8

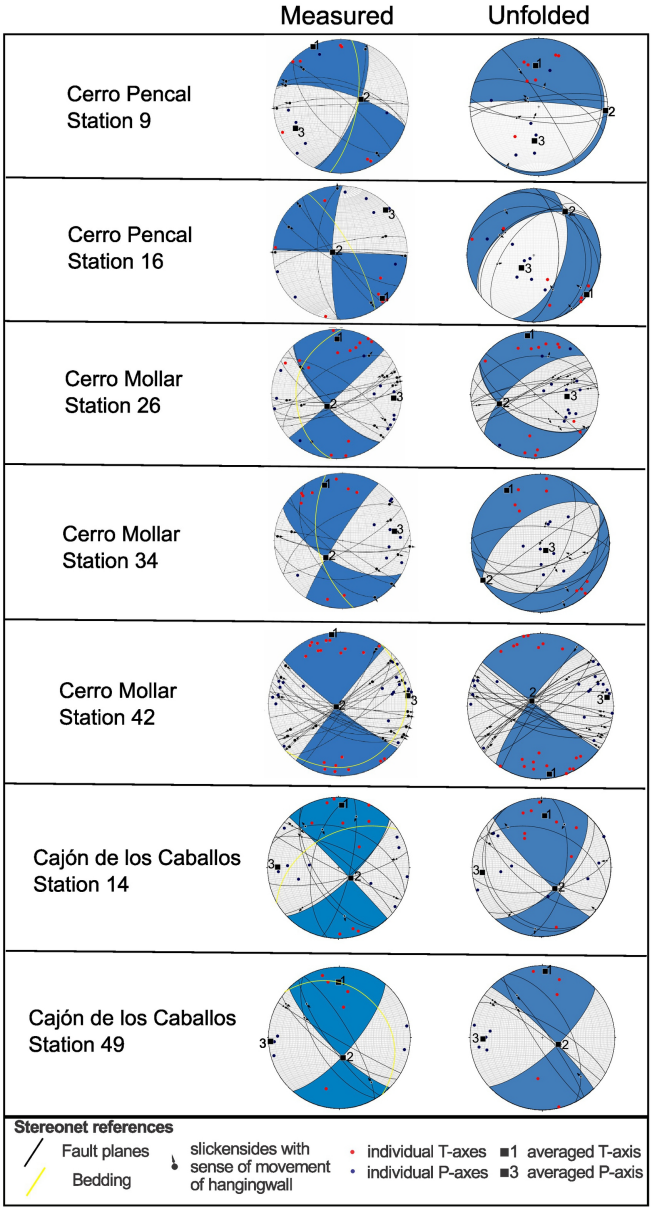
Measured
Unfolded
Cerro Pencal
Station 9
Cerro Pencal
Station 16
Cerro Mollar
Station 26
Cerro Mollar
Station 34
Cerro Mollar
Station 42
Cajón de los Caballos
Station 14
Cajón de los Caballos
Station 49
Stereonet references
Fault planes
Bedding
slickensides with
sense of movement
of hangingwall
individual T-axes
individual P-axes
1 averaged T-axis
3 averaged P-axis

Figure 9

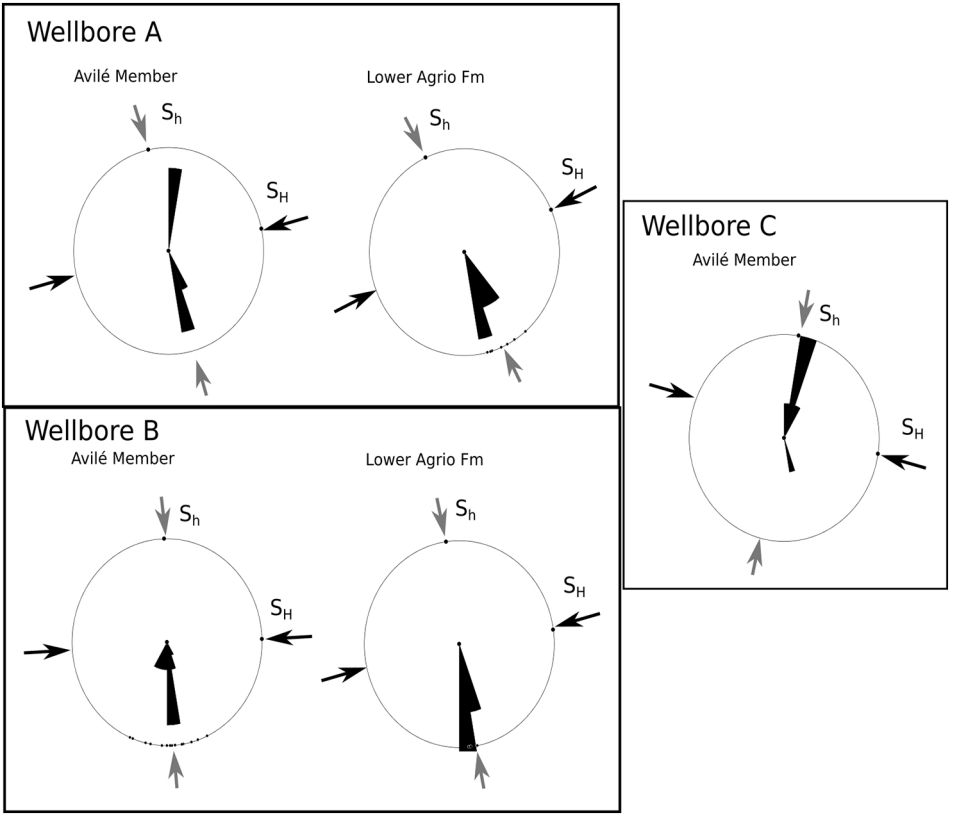
Wellbore A
Avilé Member
Lower Agrio Fm
Wellbore B
Avilé Member
Lower Agrio Fm
Wellbore C
Avilé Member
S_h
S_H

Figure 10

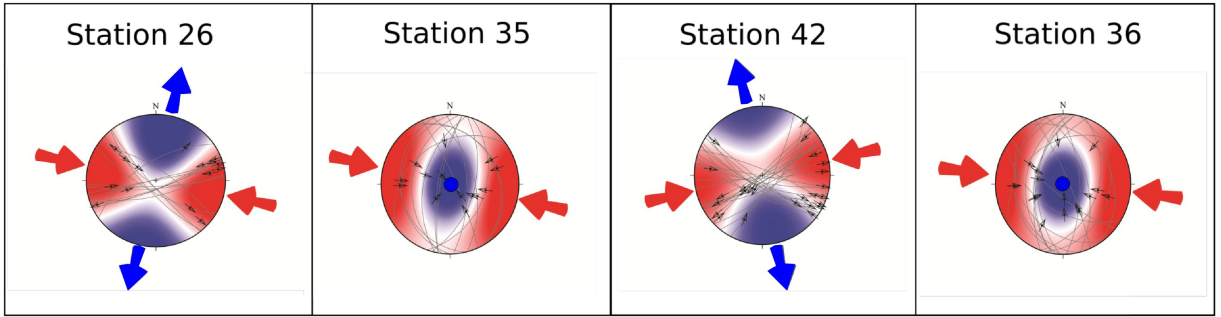

Figure 11

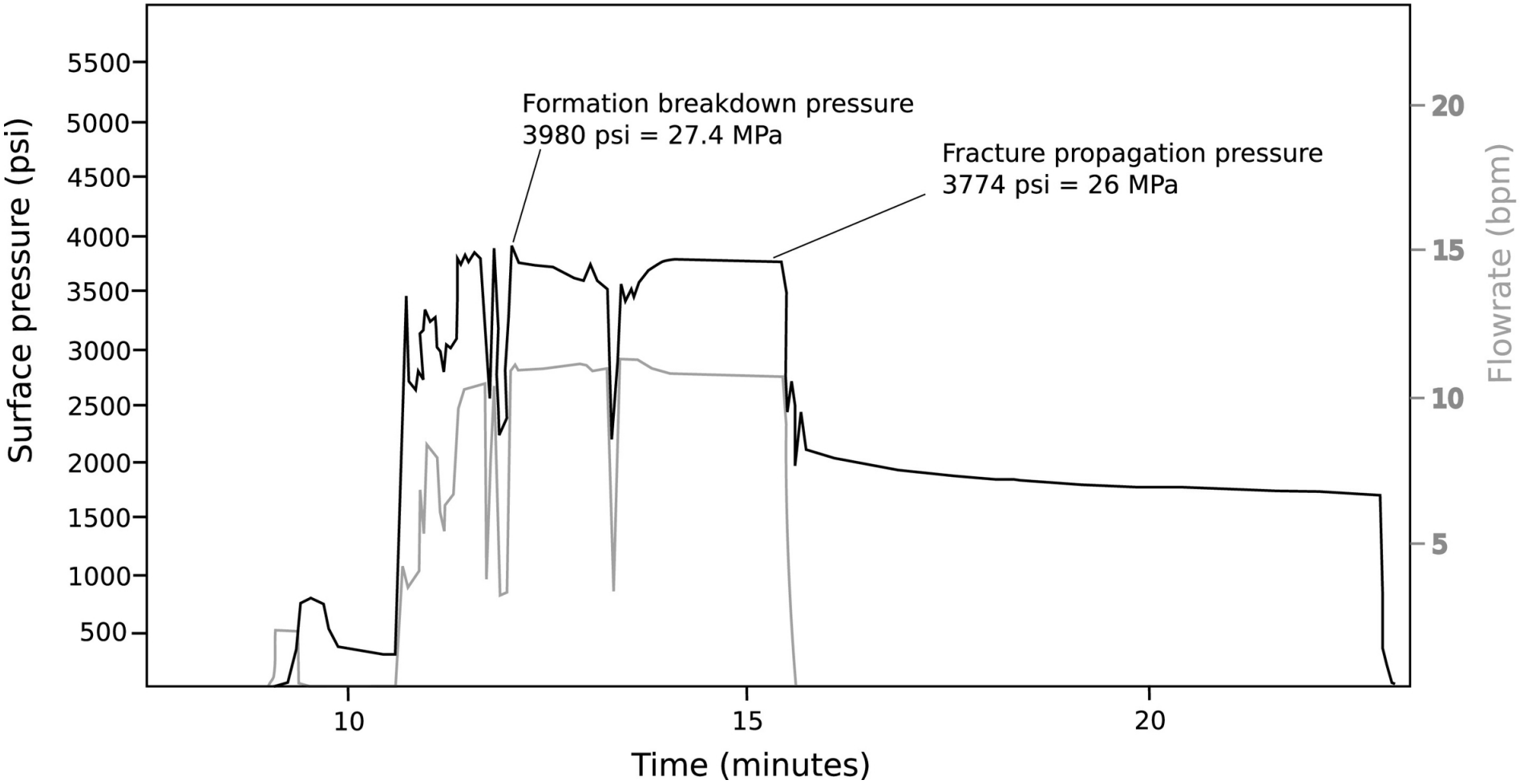
Formation breakdown pressure
3980 psi = 27.4 MPa
Fracture propagation pressure
3774 psi = 26 MPa
Surface pressure (psi)
5500
5000
4500
4000
3500
3000
2500
2000
1500
1000
500
Flowrate (bpm)
20
15
10
5
10
15
20
Time (minutes)

Figure 12

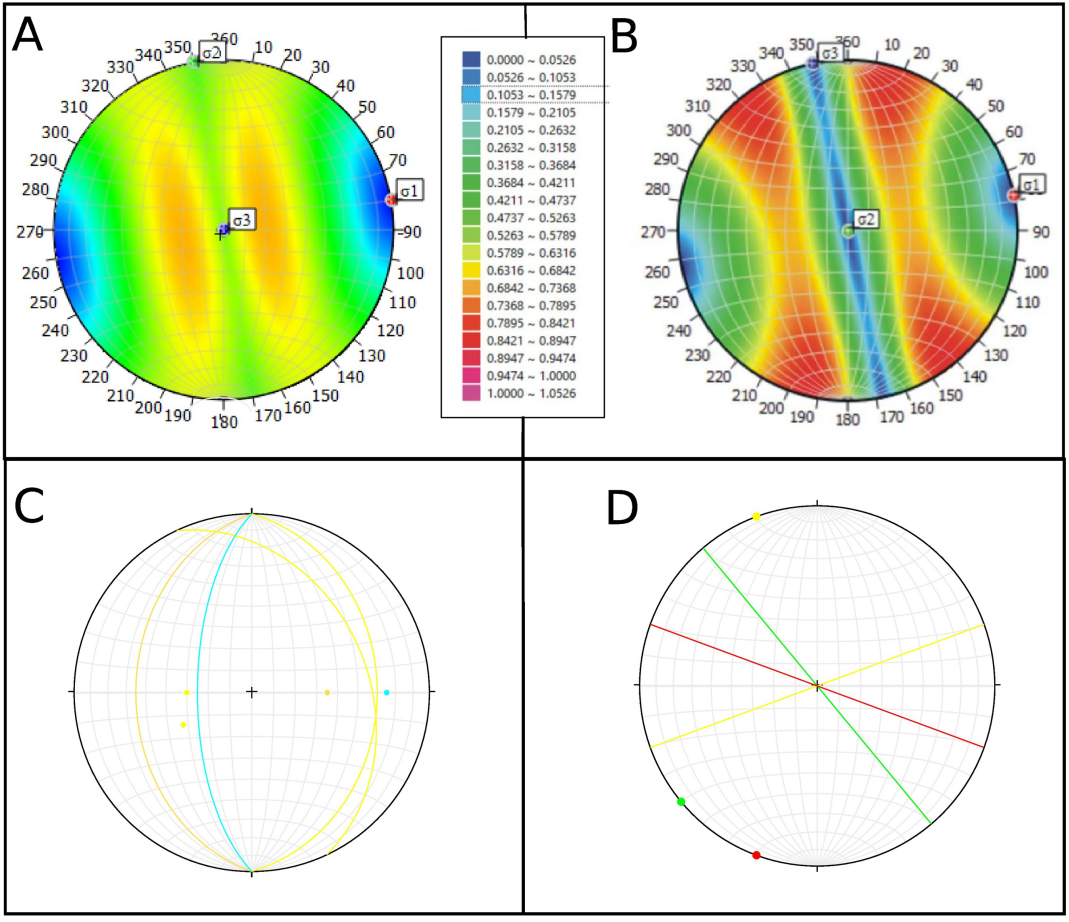
A
σ2
σ1
σ3
0.0000 ~ 0.0526
0.0526 ~ 0.1053
0.1053 ~ 0.1579
0.1579 ~ 0.2105
0.2105 ~ 0.2632
0.2632 ~ 0.3158
0.3158 ~ 0.3684
0.3684 ~ 0.4211
0.4211 ~ 0.4737
0.4737 ~ 0.5263
0.5263 ~ 0.5789
0.5789 ~ 0.6316
0.6316 ~ 0.6842
0.6842 ~ 0.7368
0.7368 ~ 0.7895
0.7895 ~ 0.8421
0.8421 ~ 0.8947
0.8947 ~ 0.9474
0.9474 ~ 1.0000
1.0000 ~ 1.0526
B
σ3
σ1
σ2
C
D

Figure 13

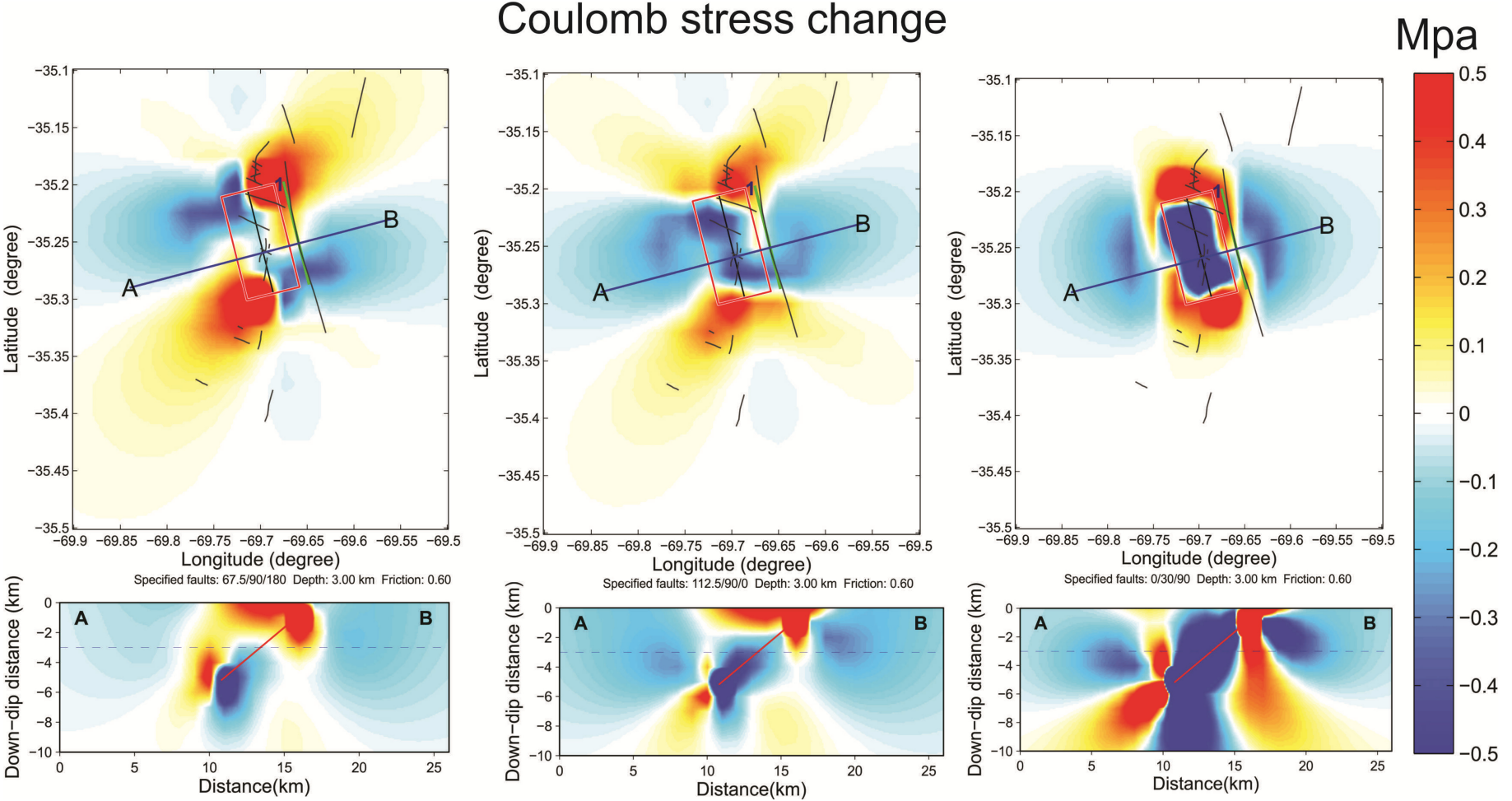
Coulomb stress change
Mpa
0.5
0.4
0.3
0.2
0.1
0
−0.1
−0.2
−0.3
−0.4
−0.5
Latitude (degree)
Longitude (degree)
A
B
Specified faults: 67.5/90/180 Depth: 3.00 km Friction: 0.60
Specified faults: 112.5/90/0 Depth: 3.00 km Friction: 0.60
Specified faults: 0/30/90 Depth: 3.00 km Friction: 0.60
Down−dip distance (km)
Distance(km)

Figure 14